Climate Dynamics (2019) 53:707–720
https://doi.org/10.1007/s00382-019-04628-0

Dynamical impact of parameterized turbulent orographic form drag on the simulation of winter precipitation over the western Tibetan Plateau

Xu Zhou[1] · Kun Yang[1,2,3] · Anton Beljaars[4] · Huidong Li[5] · Changgui Lin[6] · Bo Huang[7] · Yan Wang[2]

Received: 28 August 2018 / Accepted: 29 December 2018 / Published online: 18 January 2019

Abstract
Sub-grid orographic drag directly acts on wind and impacts the regional water cycle through control of atmospheric water vapor (AWV) transport. The effect of turbulent orographic form drag (TOFD) on wind and precipitation is investigated in this study using the WRF model for a winter month over the western Tibetan Plateau (TP), where solid precipitation supplies large amounts of water resources. The diurnal cycle of wind components and atmospheric circulation simulated with TOFD are consistent with observations and ERA-Interim data, whereas stronger westerlies exist in the simulation without the TOFD scheme. The latter results in more zonal AWV transport from the west and more precipitation over the western TP and surroundings. The implementation of the TOFD scheme leads to reduced biases, when evaluated with two observation-based precipitation products. It is therefore concluded that this scheme has a clear dynamical control on the regional atmospheric water recharge and thus the parameterization of the small-scale orographic drag in the model helps to improve the prediction of wintertime precipitation in the western TP region.

Keywords Turbulent orographic form drag · Wind · Precipitation · Tibetan Plateau · WRF

1 Introduction

Sub-grid orographic drag represents the stress of the meso to micro scale orographic variance, thus its impacts on the atmosphere are more prominent in mountainous regions than in flat areas. In numerical models, the different formulations of drag induced by the unresolved sub-grid orographic variance lead to large differences of simulated stresses over mountainous regions. Insufficient representation of sub-grid orography can lead to systematic biases in numerical weather prediction and climate models (Jimenez and Dudhia 2013; Jung and Arakawa 2016; Lee et al. 2015; Wu and Chen 1985; Zhou et al. 2017). For example, simulations of most climate models show wet and cold biases over the Tibetan Plateau (TP) such as in the study by Ji and Kang (2013) with the Regional Climate Model version 4 (RegCM4) (Giorgi et al. 2012), in 24 general circulation models of the CMIP5 project (Flato et al. 2013; Mueller and Seneviratne 2014, Su et al. 2013), and in reanalysis data e.g. NCEP-1 and ERA-40 (Feng and Zhou 2012; Gao et al. 2011; Wang and Zeng 2012), MERRA, JRA-55 and ERA-Interim (Wang and Zeng 2012). Additionally, wet biases for both long-term and seasonal simulations using WRF (Weather

✉ Kun Yang
yangk@itpcas.ac.cn

1 TEL and CETES, Institute of Tibetan Plateau Research, Chinese Academy of Sciences, 100101 Beijing, China

2 Ministry of Education Key Laboratory for Earth System Modeling, Department of Earth System Science, Tsinghua University, 10084 Beijing, China

3 University of Chinese Academy of Sciences, 100049 Beijing, China

4 European Centre for Medium-range Weather Forecasts (ECMWF), Shinfield Road, Reading RG2 9AX, UK

5 Institute of Meteorology, Freie Universität Berlin, 12165 Berlin, Germany

6 Regional Climate Group, Department of Earth Sciences, University of Gothenburg, Box 460, 405 30 Gothenburg, Sweden

7 Industrial Ecology Programme, Department of Energy and Process Engineering, Norwegian University of Science and Technology (NTNU), 7491 Trondheim, Norway

Research and Forecasting) in the TP region were also found by Gao et al. (2015) and Ma et al. (2015). Regional modeling with a finer resolution can improve the simulation of precipitation (Ji and Kang 2013; Lin et al. 2018), implying that inappropriate or lack of parameterization of the sub-grid orographic processes in a coarse-resolution model may be one of the main causes of the above biases. Therefore, parameterizations of sub-grid orographic effects are necessary in numerical models over the TP region to improve weather and climate simulations as shown in the studies of Zhou et al. (2017, 2018).

There are two groups of methods to represent the drag effect of small scale orographic features (with horizontal scales typically smaller than 5 km), namely by using (1) the effective roughness concept or (2) the distributed drag approach. Effective roughness or orographically enhanced roughness is the value of the surface roughness that should be selected in the logarithmic wind profile such that the correct enhanced drag is simulated (Fiedler and Panofsky 1972). The concept is justified by the observation that even over complex terrain far above the surface the wind profile is logarithmic and that the slope of the profile scales with friction velocity, i.e. the square root of the total surface drag divided by density (Grant and Mason 1990; Wood and Mason 1993). The effective roughness length approach is the traditional way of representing the effects of small scale orography in large scale models e.g. in the NCAR model (Neale et al. 2012). In practice it means that the transfer coefficient between the surface and the lowest model level is computed with the effective roughness rather than with the value for vegetation or land use cover. In the formulation by Jimenez and Dudhia (2012) the transfer coefficients are computed directly and not only depend on the magnitude of the sub-grid terrain variability, but also vary between valleys and peaks. An alternative approach is the distributed drag formulation where the drag is directly applied to the flow on model levels up to a certain height (Beljaars et al. 2004; Wilson 2002; Wood et al. 2001). The turbulent orographic form drag (TOFD) scheme by Beljaars et al. (2004) follows this idea and applies a scale height that is determined by the horizontal scale of the sub-grid mountains. The main difference between the effective roughness scheme and the TOFD scheme is in the height distribution of the drag: the effective roughness scheme applies drag at the lowest model level only and leaves the vertical spreading to the turbulence model. The distributed drag formulation applies drag directly to a number of model levels. In practice it also means that the effect of effective roughness length drag is strongly affected by the stability formulation of the turbulence model, whereas TOFD is much less dependent on stability.

The WRF model is widely used in meteorological (Bao et al. 2015; Guo et al. 2016; Li et al. 2017a; Norris et al. 2015; Wang et al. 2016) and hydrological (Li et al. 2017b; Zheng et al. 2016) process studies. Several schemes have been implemented in this model to account for different scales of sub-grid orographic drag, such as gravity wave and flow blocking drag (representing the orographic variance for scales larger than 3–5 km) (Choi and Hong 2015) and TOFD, representing the orographic variance with scales smaller than 5 km (Jimenez and Dudhia 2012; Lorente-Plazas et al. 2016). The above schemes for the unresolved sub-grid orography significantly contribute to the realism of global and regional wind fields and the associated atmospheric circulation (Choi et al. 2017; Choi and Hong 2015; Liang et al. 2017; Lindvall et al. 2013).

To further improve the atmospheric dynamics, the TOFD scheme, as developed by Beljaars et al. (2004), was implemented by Zhou et al. (2017, 2018) in the WRF model. The evaluation of this scheme over the TP shows a considerable improvement of 10-m wind speed. However, the atmospheric dynamical control on winter time precipitation in the Tibetan Plateau (TP) region has not been investigated yet with respect to sub-grid complex terrain, although it is expected that the dynamical processes may play an important role because the thermal forcing of the TP is weak in winter. At the same time, the above studies of Zhou et al. (2017, 2018) provide a basis of the current experimental design for model setup as described in Sect. 2.2.

The TP region controls one of the important water sources of China, India, and other Eastern Asian countries. Accurate prediction of precipitation is crucial for water source management and the local ecosystem. The TP is surrounded by high mountains with high orographic variance and the local climate is very sensitive to orographic drag. Precipitation over the TP plays an important role in controlling the regional hydrological, ecology and meteorological processes (Liu et al. 2012; Wu et al. 2012; Zhu et al. 2018; Zuo et al. 2011), but few studies focus on the western TP, where weather stations are very sparse. The goal of this study is to improve the understanding of the dynamical control of TOFD on the regional atmospheric water recharge and improve the prediction of precipitation in the western TP region.

This paper investigates the impact of TOFD on wintertime precipitation using WRF. Section 2 introduces the study area, model and methodology. The simulated 10-m and 500-hPa wind speeds (especially the diurnal cycles) with and without TOFD are evaluated in Sect. 3, which provides a basis of investigating the effects of TOFD on the simulation of precipitation through its dynamical control on atmospheric water vapor (AWV) transport (Sect. 4). Additionally, the TOFD scheme is compared with a different concept-based orographic drag scheme developed by Jimenez and Dudhia (2012, see also Lorente-Plazas et al. 2016) in Sect. 5. Concluding remarks are finally given in Sect. 6.

2 Study area and methodology

2.1 Study and analysis area

The TP is selected as the study domain (Fig. 1). The climate of the TP and surroundings is generally controlled by the monsoon in summer due to its strong thermal effect and characterized by westerly wind in winter due to the southward movement of the Ferrel cell. The mean winter temperature is very low and increases from west (− 25 °C) to east (− 15 °C) (Kuang and Jiao 2016). Due to the low temperature, precipitation is generally in the form of snow. The amount of precipitation over the central and eastern TP is rather small. However, considerable amounts are observed over the western TP related to the steep topography which blocks the westerly wind (Jin and Mullens 2012, Pu et al. 2007).

Figure 1 shows the simulation domain with the terrain height color coded. The bold white rectangle includes the TP region and near surroundings, which is our main study area. The bold black rectangle indicates the western TP, where a large amount of precipitation fell during the study period, and which was therefore selected for the precipitation evaluation. The thin black rectangles indicate the regions for cross-section plots averaged over the zonal (solid) and meridional (dashed) direction to represent the AWV transported across the western edge of the Pamir Plateau.

2.2 Model description and configuration

In this study, WRF model version 3.7 is selected to simulate wind and precipitation in a large domain around the TP (full area in Fig. 1), 800 × 500 grid points without nesting, and a horizontal grid spacing of 0.1° (about 10 km). The model has 37 levels from the surface to the top of the atmosphere at 50 hPa. WRF was configured with the Noah land surface model (Chen and Dudhia 2001), the Yonsei University planetary boundary layer scheme (Hong et al. 2006), the RRTM scheme for long-wave and solar radiative transfer (Mlawer et al. 1997), the cloud microphysics scheme by Lin et al. (1983) and the Grell 3D cumulus convection parameterization (Grell 1993). The latter is an improved version of the scheme, described by Grell and Devenyi (2002).

In order to represent the dynamical effect of small scale sub-grid orographic height variability, the TOFD scheme developed by Beljaars et al. (2004) was applied in this study. Zhou et al. (2018) implemented this scheme in the WRF model and demonstrated that considerable improvement in the simulations of wind and 2 m air temperature could be achieved. The TOFD scheme was incorporated independent of other physical schemes (e.g. the PBL and land surface schemes). It accounts for drag caused by turbulence-scale orography, with horizontal scales typically smaller than 5 km. It is implemented as a wind tendency due to a vertical stress divergence in addition to surface drag due to the land surface roughness. It does not depend on atmospheric stability and the current parameterization is applicable when the resolution is larger than 5 km. For finer model resolutions,

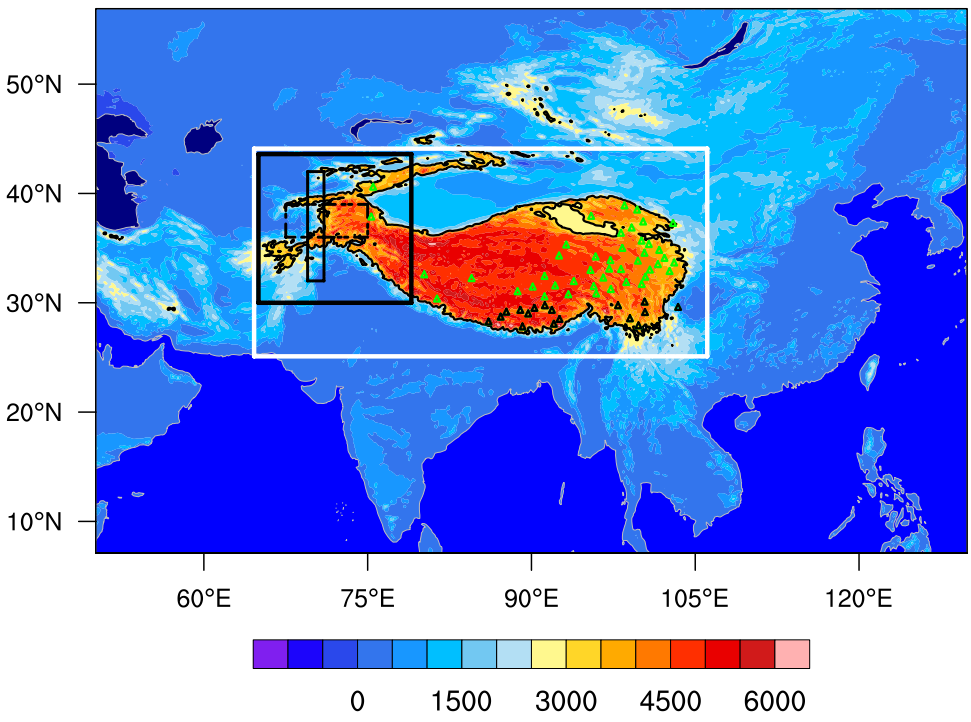

Fig. 1 Geographical distribution of the topography (color shaded; unit: m) of the simulation domain. Black triangles show the 17 stations in the southern TP and the green triangles indicate the 44 stations in the interior area of the TP. The thin black contour line represents 3000-m terrain height. The large white and large black rectangles, covering the entire TP and the western TP (Pamir Plateau plus surroundings) respectively, are selected areas for further analysis. The thin black/white solid and dashed lines indicate the regions used for cross-section averaging in Fig. 8

the scheme should obviously only cover the scales below the model grid scale. However, it is worth noting that the magnitude of TOFD is proportional to the variance of orographic slope, which is computed as a spectral integral of an empirical orographic power spectrum. Most of the contribution to this integral comes from the smallest scales, so changing the largest scale from say 5–1 km has only minor impact. The consequence is that TOFD drag is not very sensitive to the resolution of the simulation; although the key parameters can easily be recomputed for any resolution. More details can be found in Beljaars et al. (2004) and a summary is provided by Zhou et al. (2018). To study the sensitivity to TOFD, experiments are performed with and without this scheme (referred to as TOFD and NoTOFD). With the rather fine resolution of 0.1°, most of the orographic gravity wave generation and flow blocking is explicitly resolved in the WRF model and therefore the available sub-grid schemes for these processes are switched off (Zhou et al. 2017). This is also suggested in the WRF model User Guide (http://www2.mmm.ucar.edu/wrf/users/docs/user_guide_V3.7/ARWUsersGuideV3.7.pdf).

Note that there is a default small-scale orographic drag scheme in WRF developed by Jimenez and Dudhia (2012) (JD12 scheme hereafter). The JD12 scheme exerts the surface drag on the first model level in the momentum-conservation equation by including a factor dependent on the sub-grid scale orographic variability and mountain/valley height corrections. This scheme is atmospheric stability dependent. A considerable bias reduction for the surface wind speed has been demonstrated in the simulations over the Iberian Peninsula (Lorente-Plazas et al. 2016). Nevertheless, it shows limited improvements in the forecast skills in other meteorological fields including precipitation over the central western part of South Korea (Lee et al. 2015). Its effect on the simulated wind and precipitation over TP is discussed through a comparison with the current TOFD scheme in Sect. 5.

The 79 km (T255) ERA-Interim reanalysis data (Dee et al. 2011) at 6-h intervals is used as the initial condition and for the time dependent lateral boundary forcing. This reanalysis system is based on ECMWF's (European Centre for Medium-Range Weather Forecasts) Integrated Forecasting System (IFS) and assimilates a multitude of observations including measurements from conventional surface based stations and satellite platforms. The sea surface temperature is also taken from ERA-Interim, which is updated daily.

In the current study, the simulation period is from November 21st to December 31st in 2007. The reason that we select December of this year is that the mean precipitation (0.87 mm day^{-1}) during this period is close to the corresponding value averaged over 2002–2012 (0.84 mm day^{-1}) in our main focus region (western TP in Fig. 1) based on Global Precipitation Climatology Center (GPCC), and thus the selected month is representative for the climatology in winter. The initial 10 days prior to December 1st are treated as a spin-up period. Although the atmosphere has a predictability horizon that is much shorter than a month, in the current experiments the large scale synoptic variability is constrained by the forcing with re-analysis at the boundaries of the domain, so a single 41-day model integration is highly reproducible for the large scales. However, the more local details and particularly the divergent part of the flow are rather model and orography dependent. Experimentation with a resolution of 0.25° (about 25 km) demonstrated that individual simulations with the same model setup but slightly perturbed initial conditions by starting 2, 4, 6, 8 days later, are very close to the unperturbed simulation in terms of wind and precipitation (not shown). The reason is that (1) the evolution of the synoptic flow is very much controlled by the imposed boundaries from re-analysis and (2) the orographic effect is a dominant process in winter. Thus, a simulation with one initial time is sufficient to investigate the dynamical effects of the TOFD in winter. Additionally, the TOFD exerts a similar effect on the wind speed between the simulations with resolution of 0.25° and 0.1° (not shown).

2.3 Data for model evaluation and comparison

A range of observations is used to evaluate model simulations, namely in-situ observations, reanalysis data and remote sensing products. The wind fields are of particular importance, because they represent the atmospheric circulation and control the AWV transport. The latter is relevant for the interpretation of TOFD impact on precipitation. Wind components at 10 m above the ground are available from 61 weather stations from the China Meteorological Administration (CMA, http://data.cma.cn/data/detail/dataCode/A.0012.0001.html). The geographical locations of those stations are shown in Fig. 1. The data were measured hourly so they are highly suitable for the evaluation of the simulated diurnal cycle of wind speed. The simulation results are bilinearly interpolated to the station locations for comparison.

The monthly mean GPCC (Global Precipitation Climatology Center) and APHRODITE (Asian Precipitation Highly Resolved Observational Data Integration Towards Evaluation of water resources) precipitation products were used as reference data for model comparison. GPCC (https://climatedataguide.ucar.edu/climate-data/gpcc-global-precipitation-climatology-centre) is a global gridded gauge-analysis product derived from quality controlled station data with a horizontal resolution of 0.5° (Becker et al. 2013). APHRODITE (https://climatedataguide.ucar.edu/climate-data/aphrodite-asian-precipitation-highly-resolved-observational-data-integration-towards) is a 0.25° continental-scale daily product that contains a dense network of rain gauge data for Asia including the Himalayas, South and Southeast Asia, and mountainous areas in the Middle East (Yatagai et al. 2012). Both the GPCC and APHRODITE data include

a large number of high quality observations, which adds to the reliability of the datasets, although the variation of the number of stations per grid cell over time can be a major inhomogeneity source. In areas with very few or no rain gauge stations at all, the quality of these products is obviously reduced. The number of stations used in these two products can be found at the above given web pages.

The Moderate Resolution Imaging Spectroradiometer (MODIS) daily snow cover fraction (SCF; MOD10C1) and albedo (MCD43C3) collection 6 were used to determine the occurrence of snowfall over the TP region. The Terra 0.05 degree daily snow cover SCF product, which is available from the National Snow and Ice Data Center in Boulder, Colorado, USA (http://nsidc.org/data/MOD10CM#), was selected as a primary key for snow detection. SCF is calculated by using the regression equation by Salomonson and Appel (2004), which is based on the Normalized Difference Snow Index (NDSI) values of each observed pixel. The albedo data is the Climate Modeling Grid (CMG) Nadir Bidirectional Reflectance Distribution Function (BRDF) Adjusted Reflectance (NBAR) Product (https://lpdaac.usgs.gov/dataset_discovery/modis/modis_products_table/mcd43c3), which is a combined product of Terra and Aqua. The error of this high quality MODIS operational albedo is well below 5% at the majority of validation sites, and even the albedo values with "low quality flags" have been found to be primarily within 10% of the field data (Cescatti et al. 2012; Qin et al. 2011; Wang et al. 2010). The main error of the two MODIS products is generally caused by errors in the discrimination between surface snow cover and cloud (Hall and Riggs 2007).

3 Impact of TOFD on wind

Since TOFD directly retards the wind speed at the lowest model levels, a clear impact is expected at the 10 m level. Figure 2 displays the mean diurnal cycle of the simulated and measured wind components, and the wind speed averaged over all 61 stations on the TP (left) and averaged over the 17 stations on the southern TP (right). The 17 stations are generally located south

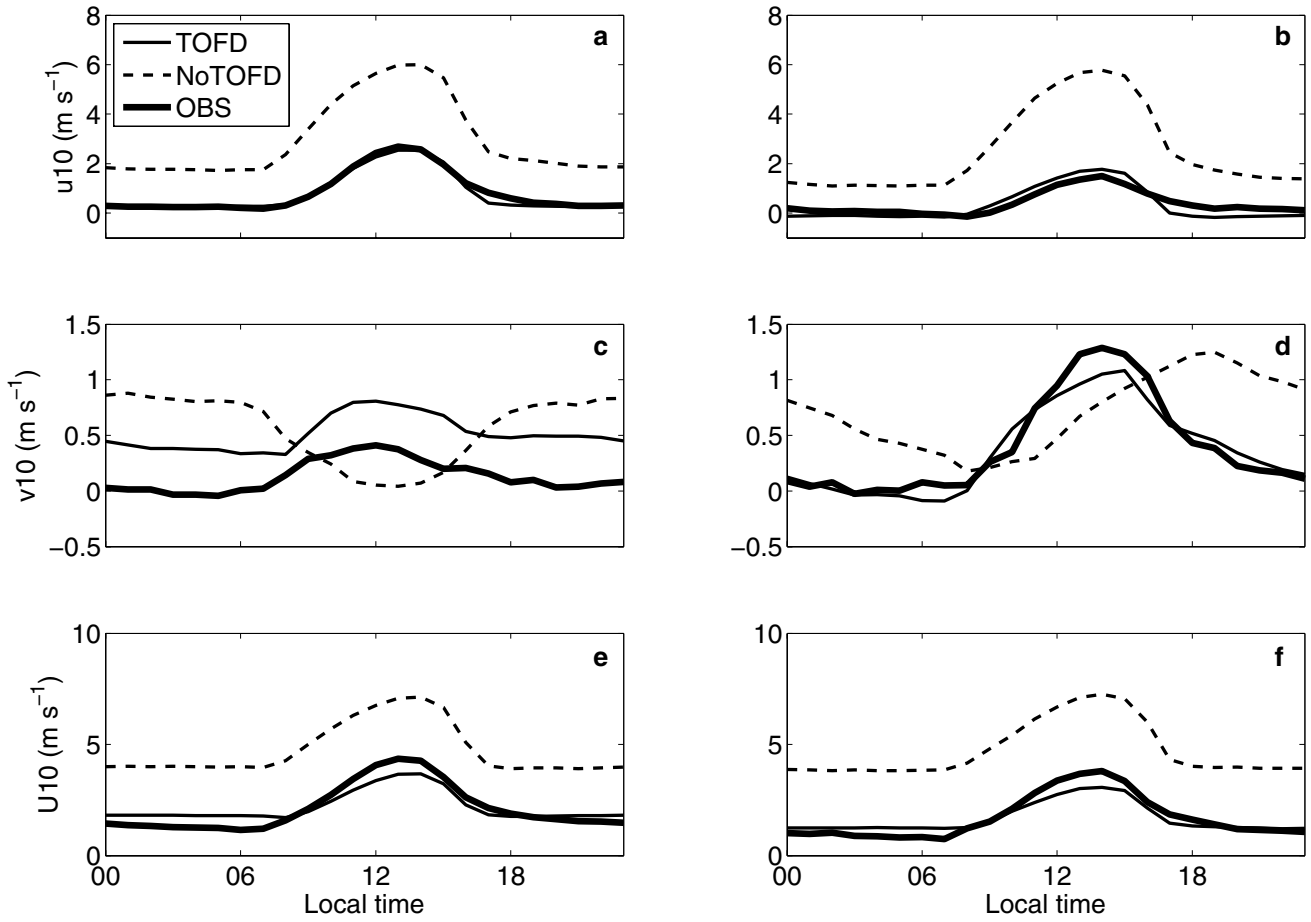

Fig. 2 Diurnal cycles of the monthly mean 10-m zonal wind (u10; unit: m s^{-1}), meridional wind (v10; unit: m s^{-1}) and total wind speed (U10; unit: m s^{-1}) derived from the TOFD run (solid), the NoTOFD run (dashed), and observations (bold) averaged over all stations in the TP (**a, c, e**) as shown in Fig. 1 (all triangles), and averaged over the stations in the southern TP (**b, d, f**; black triangles only). The study period is December 2007

of 30°N, adjacent to the Himalayan Mountains. This region generally shows high orographic variance. The TOFD run shows a reasonable magnitude of u10 (zonal wind component) and a correct pattern of the diurnal cycle of v10 (meridional wind component). In contrast, without TOFD, u10 is substantially overestimated and v10 has a diurnal cycle that is completely out of phase. The zonal wind component u10 is close to the absolute wind speed (Fig. 2e) because of the predominant westerly circulation in winter over the TP. The southern TP is adjacent to the Himalayan Mountains, and therefore, the local model climate is very sensitive to orographic drag due to its complex terrain. This is the reason that the TOFD effect on the diurnal cycle of v10 is even more pronounced over the southern TP (Fig. 2d). Moreover, this region (along the Himalaya Mountain range) is the southern boundary of the TP, through which water vapor is transported from South Asia to the interior TP.

The significant reduction in magnitude of u10 can be seen as the direct impact of more surface drag from the TOFD scheme, and the increase of the mean meridional flow is the result of the new geostrophic balance. The diurnal cycles of u10 and v10 are much more difficult to explain. Diurnal cycles of surface wind are not just the result of the day/night variation of the strength of turbulent diffusion, but also of the subtle variation with height of the diffusion coefficients. According to Monin–Obukhov similarity, turbulent diffusion coefficients decrease with height more than for neutral flow in stable situations (at night) and increase with height more rapidly than for neutral flow in unstable situations (day). The way TOFD affects the diurnal cycle is not very clear and it would require a separate single column study to explore this further.

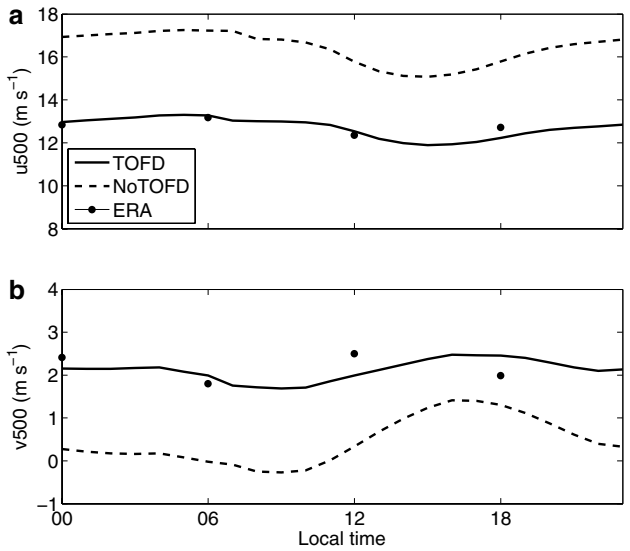

Fig. 3 Diurnal cycles of the monthly mean zonal wind (upper; unit: m^{-1}) and meridional wind (bottom; unit: m s^{-1}) at the 500 hPa pressure level in the TOFD run, NoTOFD run and the corresponding values at the specific time in the ERA-Interim dataset averaged over the entire TP region and over the study period

However, in the NoTOFD simulations, we notice that the lowest model layers are rather decoupled from the layers above, which is less the case with TOFD because of the gradually decaying function of height. This is believed to be related to the difference in diurnal cycles of NoTOFD and TOFD.

Further, the correlation coefficients of the mean diurnal v10 between the two simulations and observation have been calculated at each station. The number of stations showing positive correlation (larger than zero), namely 37 in the NoTOFD run and 46 with TOFD, also reflects the improved realism of the diurnal cycles. These results reveal that the effect of TOFD in the simulation of atmospheric dynamics is particularly strong over the mountainous southern TP region (Fig. 2).

The atmospheric flow directly controls the AWV transport between the TP and its surroundings. Impacts of the

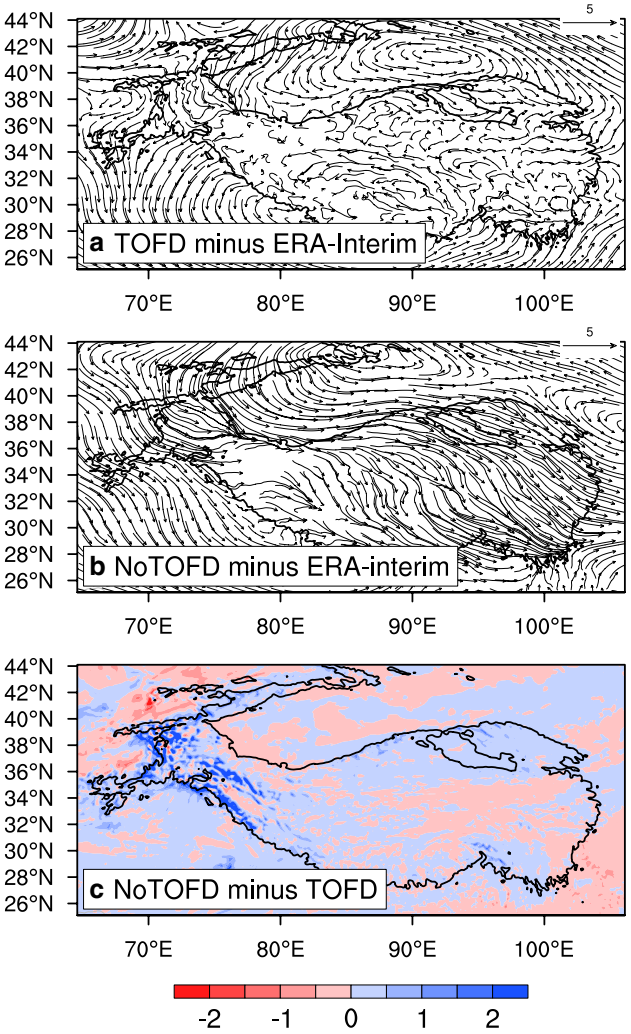

Fig. 4 Wind difference (simulation minus ERA-Interim; unit: m s^{-1}) at 500 hPa in the TOFD run (**a**) and the NoTOFD run (**b**), and the precipitation difference (mm day^{-1}) of the NoTOFD run minus the TOFD run (**c**) averaged over the study period. The black contour line shows the 3000-m terrain height

TOFD on the wind speed at 500 hPa (to represent low-level atmospheric flow) were also investigated. The diurnal cycles of the 500 hPa wind components derived from the two simulations and ERA-Interim (for specific times) are shown in Fig. 3. Generally, both runs show similar diurnal patterns. The simulation without the TOFD overestimates the u-component and underestimates the v-component at the 500 hPa surface. To illustrate the effects of the TOFD on the large-scale flow, the differences of the 500 hPa wind with respect to ERA-Interim are shown for the whole domain in Fig. 4a, b. The monthly means in this figure consist of averages of the 6-hourly fields in the study period (i.e. December 2007) as they are available from ERA-Interim. Compared to NoTOFD, TOFD simulates weaker westerlies. The above evaluation reveals that TOFD has a substantial impact on the 500 hPa flow, and that the errors with respect to surface observations and the ERA-Interim analysis (Table 1) are substantially reduced. The precipitation is expected to be influenced by the atmospheric circulation through the control of water vapor transport. Figure 4c shows the difference of precipitation between the NoTOFD run and the TOFD run. Result shows that precipitation is increased over the western TP when the TOFD scheme is switched off.

4 Impact of the TOFD on precipitation

The atmospheric flow can be seen as the dynamical link between the TP and its surrounding region. Because of its impact on the flow, TOFD modulates precipitation over the interior TP and surroundings through its dynamical control on the horizontal AWV transport. It is therefore of interest to compare precipitation in the two simulations with each other and with observations. Figure 5 shows the December mean

Table 1 The mean bias (MB; m s^{-1}), root mean square error (RMSE; m s^{-1}), and pattern correlation coefficient (CORR) of monthly mean wind speed at 10-m (versus station observation) and 500 hPa (versus ERA-Interim) in comparison with station data and the ERA-Interim analysis

Simulation	Statistic metric					
	10-m wind speed versus stations			500 hPa wind speed versus ERA-Interim		
	MB	RMSE	CORR	MB	RMSE	CORR
NoTOFD	2.61	2.84	0.45	3.15	4.30	0.45
TOFD	0.06	0.74	0.73	0.25	2.00	0.76

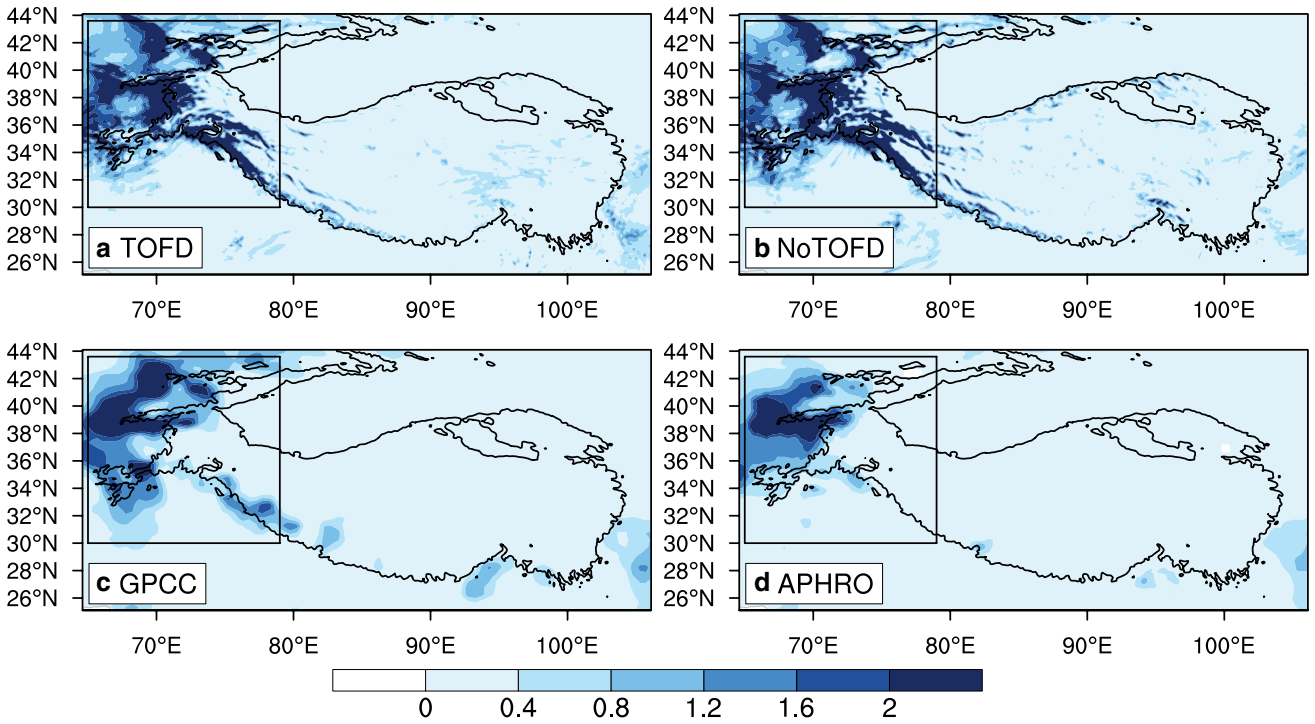

Fig. 5 Precipitation (unit: mm day^{-1}) in **a** the TOFD run, **b** the NoTOFD run, **c** GPCC data, **d** and APHRODITE (APHRO in the figure) data averaged over the study period. The black contour line shows the 3000-m terrain height; the black rectangles indicates the western TP (Pamir Plateau plus surroundings)

precipitation of the two simulations and the corresponding GPCC and APHRODITE (APHRO hereafter) data, both based on in-situ precipitation gauges. Precipitation mainly occurs over the western TP during the study period. The simulations show large amounts of precipitation over the Pamir Plateau (about 70–74°E and 35–41°N) and the western Himalaya mountain range (from about 73 to 80°E along the 3000-m terrain height contour), whereas GPCC shows much less. The APHRO data is quite similar to the GPCC product over the interior Pamir Plateau but does not have precipitation over the western Himalaya mountain range. Figure 6a, b illustrates the differences between model and observations. Overestimations in both simulations occur over the western part of Pamir Plateau and along the Himalaya Mountain range when compared with reference datasets, with NoTOFD showing larger errors. Both the GPCC and the APHRO are based on station observations and their quality can be questioned in station-sparse areas. Additionally, there are deficiencies in snowfall measurements. The reason is that instruments have systematic negative biases originating from the wind-induced gauge under-catch (Chen et al. 2015) and evaporation loss. The bias is particularly significant when little precipitation or solid precipitation occurs (Ye et al. 2004).

Satellite observations are employed to gain some insight in the uncertainty of the GPCC and APHRO data. The occurrence of precipitation can be detected by considering the change in MODIS snow cover fraction (SCF), and high albedo (Fig. 7). Precipitation is generally in the form of snowfall due to the extreme cold climate in winter. The albedo depicted by MODIS, and the MODIS SCF-change both support the large scale feature that there is much higher precipitation in GPCC and APHRO data over the western TP than the middle and eastern TP. This consistency between data sets gives confidence in the gauge based fields. Also the distribution map of precipitation gauges (see https://climatedataguide.ucar.edu/climate-data/aphrodite-asian-precipitation-highly-resolved-observational-data-integration-towards), indicates a good density of gauges in the domain of the western TP, which results in credible GPCC and APHRO data sets. Therefore statistical measures of the quality of simulated precipitation versus GPCC and APHRO data are computed (Table 2) for this area. Differences between the two reference datasets gives insight into their uncertainty: mean precipitation is 0.84 mm day^{-1} over the western TP in GPCC, while the value is 0.57 mm day^{-1} in APHRO; the root mean square difference between the two datasets

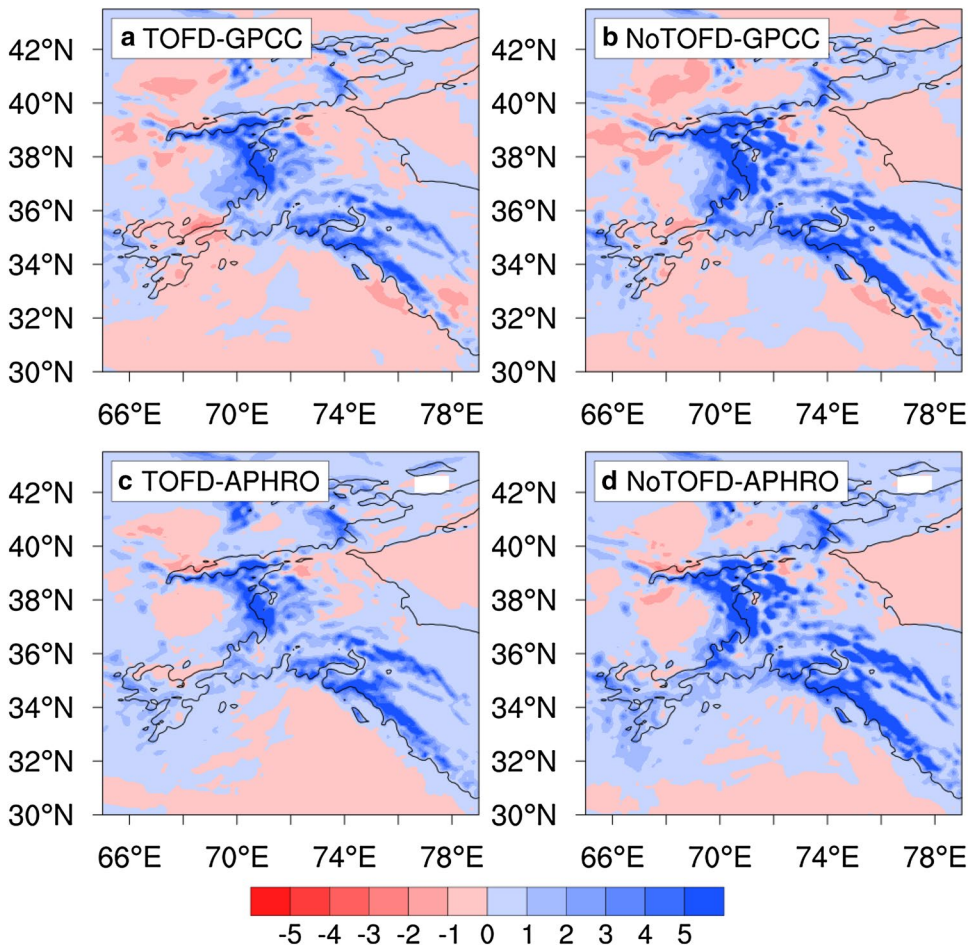

Fig. 6 Precipitation difference (mm day^{-1}) of the TOFD and NoTOFD runs minus GPCC (**a, b**) and APHRO (**c, d**) over the western TP averaged over the study period. The black contour line shows the 3000-m terrain height

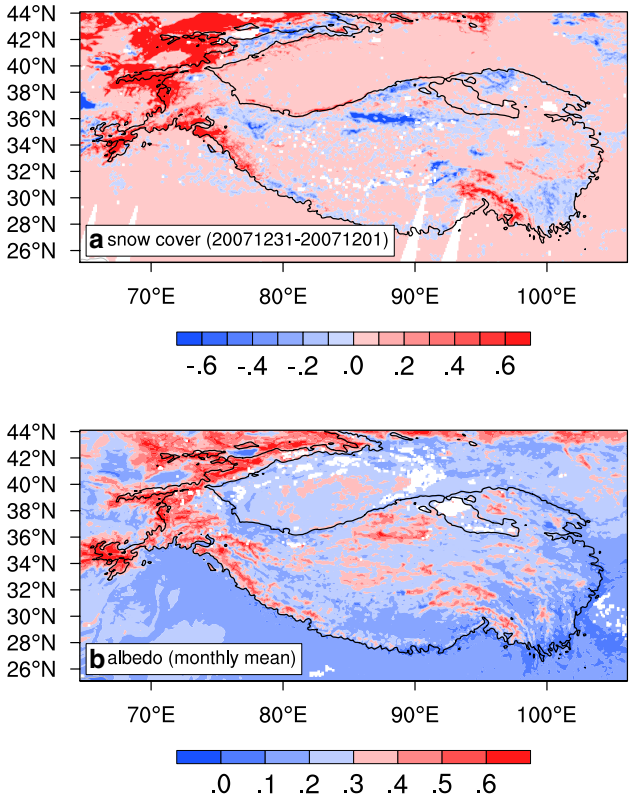

Fig. 7 MODIS snow cover fraction change indicated by the difference between the 31st and 1st of December 2007 (**a**); and MODIS monthly mean albedo for December 2007 (**b**)

is 1.16 mm day^{-1}. Nevertheless, the bias, pattern correlation, and RMS error derived from simulations versus the two datasets all support the conclusion that the TOFD run has more accurate precipitation over the western TP than the NoTOFD run.

Also for the western Himalayas there is qualitative consistency between the satellite information and GPCC, but APHRO has negligible precipitation (Fig. 5). Because MODIS SCF and albedo (Fig. 7) are more consistent with GPCC, we have more confidence in GPCC than in APHRO. The TOFD simulation is closer to GPCC than NoTOFD, but GPCC in this area is based on very few observations and therefore, it is difficult to draw firm conclusions.

Although precipitation cannot be verified everywhere to a high level of accuracy, it is of interest to interpret the differences between the two runs (Fig. 4c). The differences can be explained through AWV transport, because in winter, the ground is frozen and the evaporation/sublimation of soil water is small (Li et al. 2016). Thus, nearly all the precipitation on the plateau originates from the horizontal AWV transport. Differences (NoTOFD minus TOFD) of $\overline{uq}$ (monthly mean zonal wind multiplied by specific humidity) along a zonal cross-section and along a meridional cross-section are given in Fig. 8. The zonal flow is generally perpendicular to the western edge of the Pamir Plateau, where the AWV is transported to the interior plateau through horizontal advection. The stronger westerly in the NoTOFD run leads to more AWV transport from the west than in the TOFD run, especially at low levels (Fig. 8). This results in more precipitation over the Pamir Plateau (Fig. 4c) in NoTOFD. The above difference in AWV transport can also be seen from the 500 hPa transport difference and the vertically integrated transport differences of wind vector multiplied by specific humidity (Fig. 9). It is clear that the changed AWV flow is perpendicular to the western range of the Pamir Plateau and western Himalaya mountains, which is a direct effect of the parameterized TOFD on the atmospheric flow.

5 Discussion on the sensitivity to orographic drag schemes

According to the above analysis, the current TOFD scheme effectively reduces the precipitation amount over the western TP. Meanwhile, there is a default scheme for small-scale orographic drag in WRF, which was proposed by Jimenez and Dudhia (2012). This scheme parameterizes the drag in the surface layer and influences the wind profile in the upper layers through the vertical diffusion. Thus, an additional simulation with this scheme is performed to make a comparison (Fig. 10) with the current TOFD scheme.

Table 2 Mean precipitation (mm day^{-1}) from different datasets in the western TP (indicated by large black rectangles in Fig. 1), and the mean bias (MB; mm day^{-1}), root mean square error (RMSE; mm day^{-1}), and pattern correlation coefficient (CORR) for simulated precipitation versus reference data (GPCC and APHRODITE)

Simulation	Statistic metric						
	Mean precipitation	Simulation versus GPCC			Simulation versus APHRO		
		MB	RMSE	CORR	MB	RMSE	CORR
GPCC/APHRO	0.84/0.57	–	–	–	–	–	–
NoTOFD	1.54	0.69	2.20	0.31	0.97	2.25	0.39
TOFD	1.22	0.38	1.40	0.49	0.66	1.46	0.55

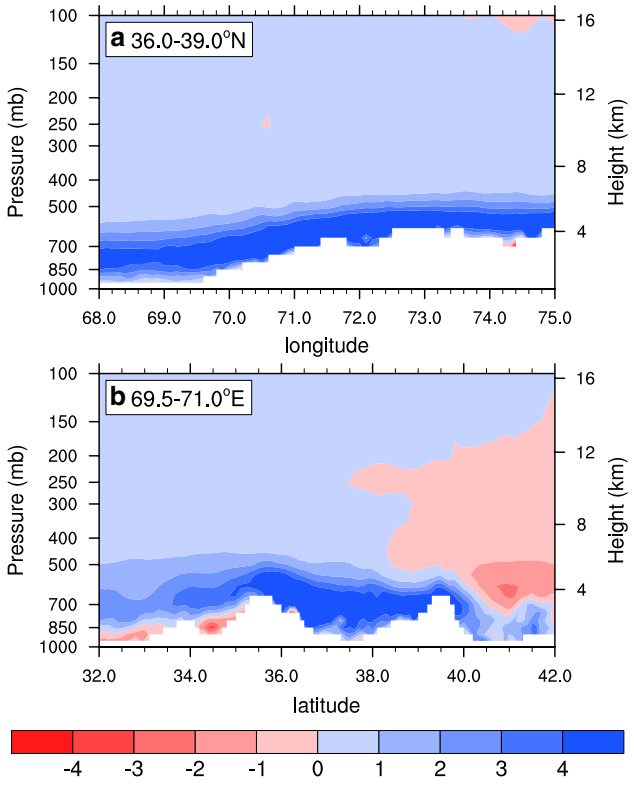

Fig. 8 Differences (NoTOFD minus TOFD) of $\overline{uq}$ ($g{\cdot}kg^{-1}{\cdot}m{\cdot}s^{-1}$; zonal wind multiplied by specific humidity) at the western edge of the Pamir Plateau **a** along a zonal cross-section averaged over 36–39°N (Fig. 1, thin solid black line), and **b** along a meridional cross-section averaged over 69.5–71°E (Fig. 1, thin dashed black line). The average is performed only for the grid points above the ground

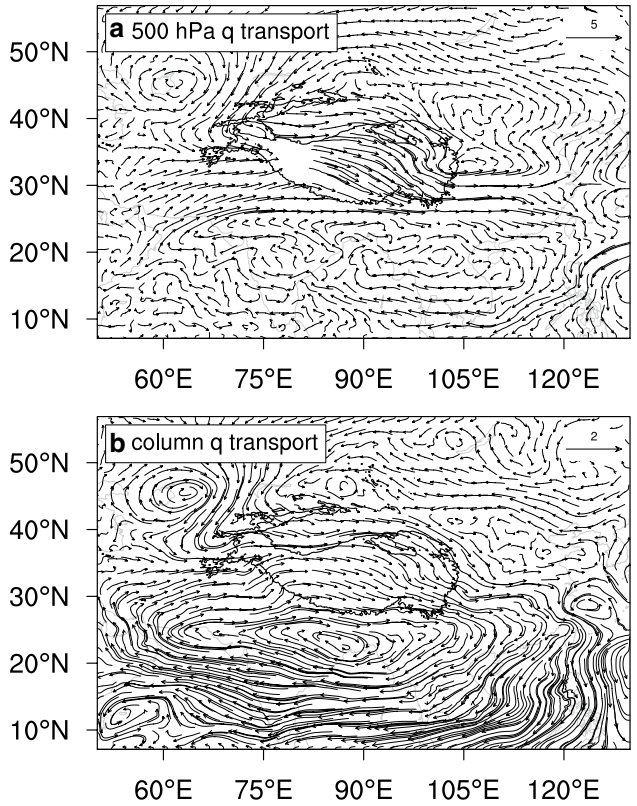

Fig. 9 The difference of $\vec{V}q$ ($g{\cdot}kg^{-1}{\cdot}m{\cdot}s^{-1}$) at 500 hPa and vertically integrated $\vec{V}q$ from the bottom to the top of the atmosphere (50 hPa; 10^4 $g{\cdot}m^{-1}{\cdot}s^{-1}$) derived from the NoTOFD minus TOFD runs averaged over the study period. The black contour line shows the 3000-m terrain height

As shown in Fig. 10a, the implementation of the JD12 scheme also effectively reduces the zonal wind speed, but the magnitude of the reduction is less and its bias is greater than that with the current TOFD scheme. The diurnal pattern of the mean meridional wind in the JD12 run is similar to the NoTOFD run which is opposite to the observed one (Fig. 10b). This indicates that the current TOFD scheme performs better than the default JD12 scheme in simulating the 10-m wind speed, which is believed to be associated with the large scale circulation. The current TOFD scheme has stronger effects on the upper-layer atmospheric flow than JD12 does (Fig. 10c, d) due to the fact that the former adds the orographic drag at each model layer following an exponential decay with altitude while the JD12 scheme modulates the drag at the lowest model level only. This is consistent with the statement in Liang et al. (2017) that the currently used TOFD scheme is more sensitive to complex orography. As a result, the impact on the large scale circulation by the JD12 scheme is not strong enough to correct the diurnal cycle in v10. Meanwhile, JD12 has a weaker dynamical control on the AWV transport (not shown) and its effects on the simulation of precipitation are limited compared with the current TOFD scheme (see Fig. 10e, f).

6 Concluding remarks

In the current study, the impacts of a turbulent orographic form drag (TOFD) scheme on precipitation over the western TP winter were investigated based on WRF simulations. The WRF simulation produces reasonable diurnal cycles of wind speed (especially over the southern TP) and regional atmospheric circulation when the TOFD scheme proposed by Beljaars et al. (2004) is included, whereas the simulation without the TOFD scheme has too strong westerlies. Accordingly, the former case yields less water vapor advection to the western TP due to the weakened westerly wind, which results in less bias in precipitation than the latter case.

There are alternative schemes to represent sub-grid orographic drag [e.g. the JD12 scheme in WRF and the turbulent mountain stress scheme in the National Center for Atmospheric Research Community Earth System

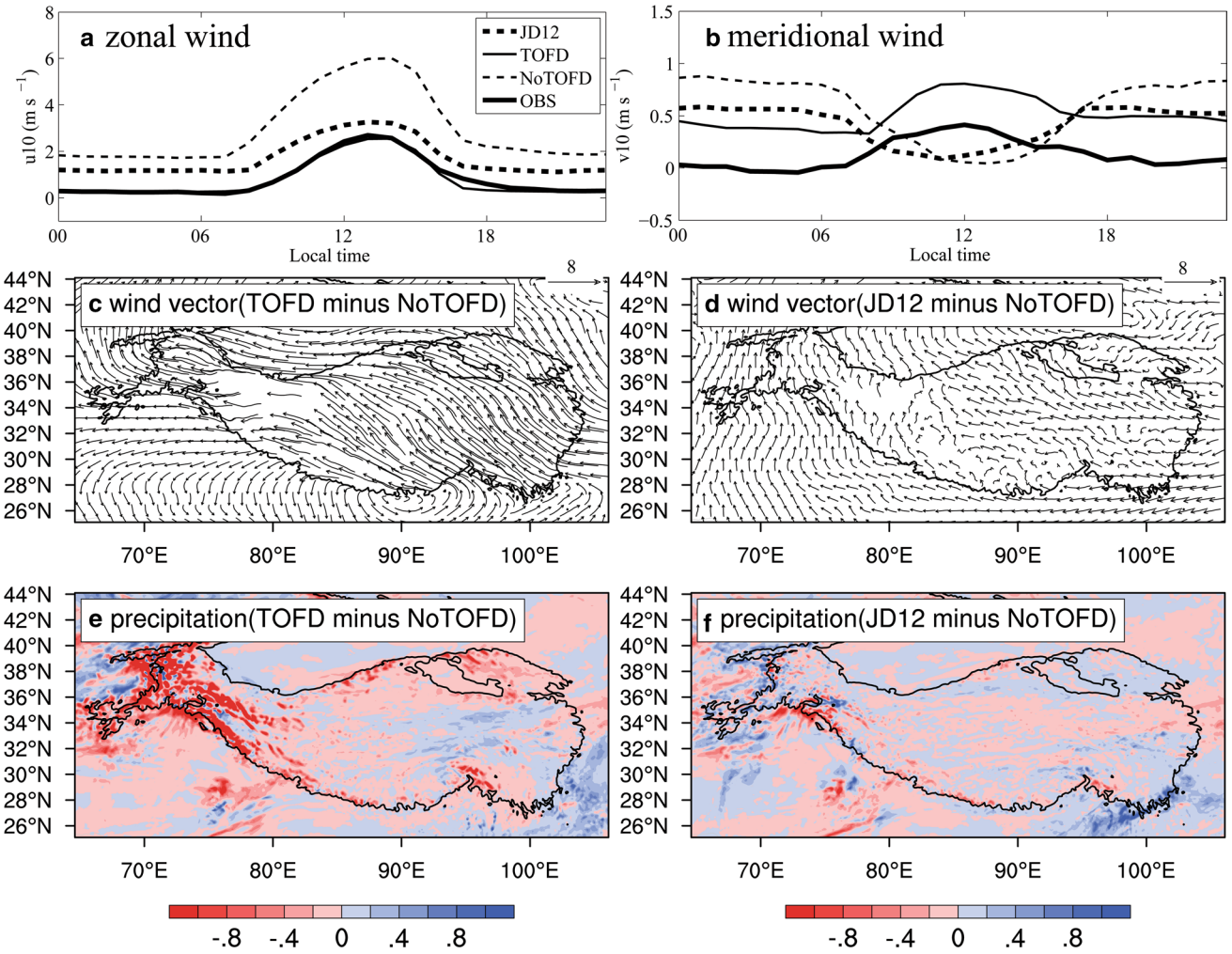

Fig. 10 Comparisons of diurnal cycles of 10-m wind components (**a, b**; m s^{-1}); the difference in 500-hPa atmospheric wind (m s^{-1}) derived from the TOFD run minus the NoTOFD run (**c**) and that from the JD12 run minus the NoTOFD run (**d**); and the difference in precipitation (mm day^{-1}) derived from the TOFD run minus the NoTOFD run (**e**) and that from the JD12 run minus the NoTOFD run (**f**)

Model (Neale et al. 2012)]. These schemes all have the inherent characteristic of obstructing the horizontal atmospheric flow. In this study, we compared the JD12 scheme, a default one in WRF, with the TOFD scheme in terms of the simulation of wind speed and precipitation. It is shown that the JD12 scheme can effectively reduce the wind speed over the TP during winter, but its performance is poorer than the TOFD scheme, in terms of wind speed magnitude and its diurnal pattern. The difference in performance is related to their structure: the JD12 scheme adds the orographic drag at the lowest atmosphere level only, whereas the TOFD scheme adds the drag at each level following an exponential decay with height. The latter results in a much stronger modulation of the large-scale circulation. Nevertheless, inter-comparisons of multiple schemes for sub-grid orographic drag are highly desirable, as proposed in the "Drag project" (Zadra 2013), which was initiated by the Working Group for Numerical Experimentation of the World Meteorological Organization.

As far as we know, this study is the first to investigate the impact of small scale orographic drag on the simulation of wintertime precipitation in the TP. Our result highlights the distinct dynamical control of the parameterized sub-grid orographic drag (especially this TOFD scheme) on the regional atmospheric water recharge and its importance in wintertime snowfall simulations for this unique region.

This work together with previous work by Zhou et al. (2018) show that the incorporation of small-scale orographic drag can effectively improve the simulation of precipitation over the TP region both in winter and summer. Thus, large scale and long period simulations are expected to benefit from the inclusion of sub-grid orographic drag parameterizations. However, the simulated

precipitation is still biased, especially when the thermal effect is strong. TOFD can reduce only about 20% of the precipitation bias compared to station averages in summer (Zhou et al. 2018). The reason could be that the sub-grid orographic variance not only has dynamic barrier effects but also influences the atmospheric circulation and synoptic conditions through thermal effects (e.g. associated with clouds, radiation and turbulent heat fluxes) (Feng and Zhang 2007; Zhang et al. 2006). These thermal effects also need accurate representations in numerical weather prediction and climate models.

Acknowledgements The simulations were performed at the HPCC super-computer at the Institute of Tibetan Plateau Research. The station data was provided by National Meteorological Information Center, China Meteorological Administration. The ERA-Interim reanalysis data was downloaded from https://www.ecmwf.int/en/forecasts/datasets. We are grateful to the China Meteorological Administration and ECMWF for offering the necessary data.

Funding This work was funded by the National Key Research and Development Program of China (Grant no. 2018YFA0605400), the National Natural Science Foundation of China (Grant nos. 41705084, 91537210), the Key Frontier Project of Chinese Academy of Sciences (Grant no. QYZDY-SSW-DQC011-03), and the National Key Basic Research Program of China (Grant no. 2015CB953703).

Compliance with ethical standards

Conflict of interest There is no conflict of interests for any author.

References

Bao JW, Feng JM, Wang YL (2015) Dynamical downscaling simulation and future projection of precipitation over China. J Geophys Res-Atmos 120(16):8227–8243. https://doi.org/10.1002/2015jd023275

Becker A, Finger P, Meyer-Christoffer A, Rudolf B, Schamm K, Schneider U, Ziese M (2013) A description of the global land-surface precipitation data products of the Global Precipitation Climatology Centre with sample applications including centennial (trend) analysis from 1901-present. Earth Syst Sci Data 5(1):71–99. https://doi.org/10.5194/essd-5-71-2013

Beljaars ACM, Brown AR, Wood N (2004) A new parametrization of turbulent orographic form drag. Q J R Meteor Soc 130(599):1327–1347. https://doi.org/10.1256/qj.03.073

Cescatti A et al (2012) Intercomparison of MODIS albedo retrievals and in situ measurements across the global FLUXNET network. Remote Sens Environ 121:323–334. https://doi.org/10.1016/j.rse.2012.02.019

Chen, F., and J. Dudhia (2001), Coupling an advanced land surface-hydrology model with the Penn State-NCAR MM5 modeling system. Part II: preliminary model validation. Mon Weather Rev 129(4):587–604. https://doi.org/10.1175/1520-0493(2001)129%3C0587:Caalsh%3E2.0.Co;2.

Chen R, Liu J, Kang E, Yang Y, Han C, Liu Z, Song Y, Qing W, Zhu P (2015) Precipitation measurement intercomparison in the Qilian Mountains, north-eastern Tibetan Plateau. Cryosphere 9(5):1995–2008. https://doi.org/10.5194/tc-9-1995-2015

Choi HJ, Hong SY (2015) An updated subgrid orographic parameterization for global atmospheric forecast models. J Geophys Res-Atmos 120(24):12445–12457. https://doi.org/10.1002/2015jd024230

Choi HJ, Choi SJ, Koo MS, Kim JE, Kwon YC, Hong SY (2017) Effects of parameterized orographic drag on weather forecasting and simulated climatology over East Asia during boreal summer. J Geophys Res-Atmos 122(20):10669–10678. https://doi.org/10.1002/2017jd026696

Dee DP et al (2011) The ERA-Interim reanalysis: configuration and performance of the data assimilation system. Q J R Meteor Soc 137(656):553–597. https://doi.org/10.1002/qj.828

Feng L, Zhang Y (2007) Impacts of the thermal effects of sub-grid orography on the heavy rainfall events along the Yangtze river valley in 1991. Adv Atmos Sci 24(5):881–892. https://doi.org/10.1007/s00376-007-0881-4

Feng L, Zhou TJ (2012) Water vapor transport for summer precipitation over the Tibetan Plateau: multidata set analysis. J Geophys Res-Atmos 117:D20. https://doi.org/10.1029/2011jd017012

Fiedler F, Panofsky H (1972) The geostrophic drag coefficient and the effective roughness length. Q J R Meteor Soc 98(415):213–220. https://doi.org/10.1002/qj.49709841519

Flato G, Marotzke J, Abiodun B, Braconnot P, Chou S, Collins W, Cox P, Driouech F (2013) Contribution of working group I to the Fifth assessment report of the intergovernmental panel on climate change. Clim Change 2013(5):741–866

Gao YH, Xue YK, Peng W, Kang HS, Waliser D (2011) Assessment of dynamic downscaling of the extreme rainfall over East Asia using a regional climate model. Adv Atmos Sci 28(5):1077–1098. https://doi.org/10.1007/s00376-010-0039-7

Gao YH, Xu JW, Chen DL (2015) Evaluation of WRF mesoscale climate simulations over the Tibetan Plateau during 1979–2011. J Clim 28(7):2823–2841. https://doi.org/10.1175/Jcli-D-14-00300.1

Giorgi F et al (2012) RegCM4: model description and preliminary tests over multiple CORDEX domains. Clim Res 52(1):7–29. https://doi.org/10.3354/cr01018

Grant ALM, Mason PJ (1990) Observations of boundary-layer structure over complex terrain. Q J R Meteor Soc 116(491):159–186

Grell GA (1993) Prognostic evaluation of assumptions used by cumulus parameterizations. Mon Weather Rev 121(3):764–787. https://doi.org/10.1175/1520-0493(1993)121%3C0764:Peoaub%3E2.0.Co;2.

Grell GA, Devenyi D (2002) A generalized approach to parameterizing convection combining ensemble and data assimilation techniques. Geophys Res Lett 29:14. https://doi.org/10.1029/2002gl015311

Guo DL, Yu ET, Wang HJ (2016) Will the Tibetan Plateau warming depend on elevation in the future? J Geophys Res-Atmos 121(8):3969–3978. https://doi.org/10.1002/2016jd024871

Hall DK, Riggs GA (2007) Accuracy assessment of the MODIS snow products. Hydrol Process 21(12):1534–1547. https://doi.org/10.1002/hyp.6715

Hong SY, Noh Y, Dudhia J (2006) A new vertical diffusion package with an explicit treatment of entrainment processes. Mon Weather Rev 134(9):2318–2341. https://doi.org/10.1175/Mwr3199.1

Ji ZM, Kang SC (2013) Double-nested dynamical downscaling experiments over the Tibetan Plateau and their projection of climate change under two RCP scenarios. J Atmos Sci 70(4):1278–1290. https://doi.org/10.1175/Jas-D-12-0155.1

Jimenez PA, Dudhia J (2012) Improving the representation of resolved and unresolved topographic effects on surface wind in the WRF model. J Appl Meteorol Clim 51(2):300–316. https://doi.org/10.1175/Jamc-D-11-084.1

Jimenez PA, Dudhia J (2013) On the ability of the WRF model to reproduce the surface wind direction over complex terrain. J Appl Meteorol Clim 52(7):1610–1617. https://doi.org/10.1175/Jamc-D-12-0266.1

Jin MS, Mullens TJ (2012) Land-biosphere-atmosphere interactions over the Tibetan Plateau from MODIS observations. Environ Res Lett 7:1. https://doi.org/10.1088/1748-9326/7/1/014003

Jung JH, Arakawa A (2016) Simulation of subgrid orographic precipitation with an embedded 2-D cloud-resolving model. J Adv Model Earth Sy 8(1):31–40. https://doi.org/10.1002/2015ms000539

Kuang XX, Jiao JJ (2016) Review on climate change on the Tibetan Plateau during the last half century. J Geophys Res-Atmos 121(8):3979–4007. https://doi.org/10.1002/2015jd024728

Lee J, Shin HH, Hong SY, Jimenez PA, Dudhia J, Hong J (2015) Impacts of subgrid-scale orography parameterization on simulated surface layer wind and monsoonal precipitation in the high-resolution WRF model. J Geophys Res-Atmos 120(2):644–653. https://doi.org/10.1002/2014jd022747

Li HD, Wang AZ, Guan DX, Jin CJ, Wu JB, Yuan FH, Shi TT (2016), Empirical model development for ground snow sublimation beneath a temperate mixed forest in Changbai mountain. J Hydrol Eng 21:11. https://doi.org/10.1061/(Asce)He.1943-5584.0001415

Li HD, Wolter M, Wang X, Sodoudi S (2018) Impact of land cover data on the simulation of urban heat island for Berlin using WRF coupled with bulk approach of Noah-LSM. Theor Appl Climatol 134:67–81. https://doi.org/10.1007/s00704-017-2253-z

Li L, Gochis DJ, Sobolowski S, Mesquita MDS (2017b) Evaluating the present annual water budget of a Himalayan headwater river basin using a high-resolution atmosphere-hydrology model. J Geophys Res-Atmos 122(9):4786–4807. https://doi.org/10.1002/2016jd026279

Liang YS, Wang LN, Zhang GJ, Wu QZ (2017) Sensitivity test of parameterizations of subgrid-scale orographic form drag in the NCAR CESM1. Clim Dyn 48(9–10):3365–3379. https://doi.org/10.1007/s00382-016-3272-7

Lin YL, Farley RD, Orville HD (1983) Bulk parameterization of the snow field in a cloud model. J Clim Appl Meteorol 22(6):1065–1092. https://doi.org/10.1175/1520-0450(1983)022<1065:BPOTSF>2.0.CO;2

Lin CG, Chen DL, Yang K, Ou TH (2018) Impact of model resolution on simulating the water vapor transport through the central Himalayas: implication for models' wet bias over the Tibetan Plateau. Clim Dyn. https://doi.org/10.1007/s00382-018-4074-x

Lindvall J, Svensson G, Hannay C (2013) Evaluation of near-surface parameters in the two versions of the atmospheric model in CESM1 using flux station observations. J Clim 26(1):26–44. https://doi.org/10.1175/Jcli-D-12-00020.1

Liu YM, Wu GX, Hong JL, Dong BW, Duan AM, Bao Q, Zhou LJ (2012) Revisiting Asian monsoon formation and change associated with Tibetan Plateau forcing: II. Change. Clim Dyn 39(5):1183–1195. https://doi.org/10.1007/s00382-012-1335-y

Lorente-Plazas R, Jimenez PA, Dudhia J, Montavez JP (2016) Evaluating and improving the impact of the atmospheric stability and orography on surface winds in the WRF model. Mon Weather Rev 144(7):2685–2693. https://doi.org/10.1175/Mwr-D-15-0449.1

Ma JH, Wang HJ, Fan K (2015) Dynamic downscaling of summer precipitation prediction over China in 1998 using WRF and CCSM4. Adv Atmos Sci 32(5):577–584. https://doi.org/10.1007/s00376-014-4143-y

Mlawer EJ, Taubman SJ, Brown PD, Iacono MJ, Clough SA (1997) Radiative transfer for inhomogeneous atmospheres: RRTM, a validated correlated-k model for the longwave. J Geophys Res-Atmos 102(D14):16663–16682. https://doi.org/10.1029/97jd00237

Mueller B, Seneviratne SI (2014) Systematic land climate and evapotranspiration biases in CMIP5 simulations. Geophys Res Lett 41(1):128–134. https://doi.org/10.1002/2013gl058055

Neale RB et al (2012) Description of the NCAR community atmosphere model (CAM 5.0), NCAR technical note, pp 106–107

Norris J, Carvalho LMV, Jones C, Cannon F (2015) WRF simulations of two extreme snowfall events associated with contrasting extratropical cyclones over the western and central Himalaya. J Geophys Res-Atmos 120(8):3114–3138. https://doi.org/10.1002/2014jd022592

Pu ZX, Xu L, Salomonson VV (2007), MODIS/Terra observed seasonal variations of snow cover over the Tibetan Plateau. Geophys Res Lett 34:6. https://doi.org/10.1029/2006gl029262

Qin J, Yang K, Liang SL, Zhang H, Ma YM, Guo XF, Chen ZQ (2011) Evaluation of surface albedo from GEWEX-SRB and ISCCP-FD data against validated MODIS product over the Tibetan Plateau. J Geophys Res-Atmos 116:D24. https://doi.org/10.1029/2011jd015823

Salomonson VV, Appel I (2004) Estimating fractional snow cover from MODIS using the normalized difference snow index. Remote Sens Environ 89(3):351–360. https://doi.org/10.1016/j.rse.2003.10.016

Su FG, Duan XL, Chen DL, Hao ZC, Cuo L (2013) Evaluation of the global climate models in the CMIP5 over the Tibetan Plateau. J Clim 26(10):3187–3208. https://doi.org/10.1175/Jcli-D-12-00321.1

Wang AH, Zeng XB (2012) Evaluation of multireanalysis products with in situ observations over the Tibetan Plateau. J Geophys Res-Atmos 117:D5. https://doi.org/10.1029/2011jd016553

Wang KC, Liang S, Schaaf CL, Strahler AH (2010) Evaluation of moderate resolution imaging spectroradiometer land surface visible and shortwave albedo products at FLUXNET sites. J Geophys Res-Atmos 115:D17. https://doi.org/10.1029/2009jd013101

Wang AM, Duan MS, Li, He B (2016) Influences of thermal forcing over the slope/platform of the Tibetan Plateau on Asian summer monsoon: numerical studies with the WRF model. Chin J Geophys 59(9):3175–3187. https://doi.org/10.6038/cjg20160904

Wilson JD (2002) Representing drag on unresolved terrain as a distributed momentum sink. J Atmos Sci 59(9):1629–1637. https://doi.org/10.1175/1520-0469(2002)059%3C1629:Rdouta%3E2.0.Co;2

Wood N, Mason P (1993) The pressure force induced by neutral, turbulent-flow over hills. Q J R Meteor Soc 119(514):1233–1267. https://doi.org/10.1002/qj.49711951402

Wood N, Brown AR, Hewer FE (2001) Parametrizing the effects of orography on the boundary layer: an alternative to effective roughness lengths. Q J R Meteor Soc 127(573):759–777. https://doi.org/10.1256/smsqj.57302

Wu GX, Chen SJ (1985) The effect of mechanical forcing on the formation of a mesoscale vortex. Q J R Meteor Soc 111(470):1049–1070. https://doi.org/10.1256/smsqj.47008

Wu GX, Liu YM, Dong BW, Liang XY, Duan AM, Bao Q, Yu JJ (2012) Revisiting Asian monsoon formation and change associated with Tibetan Plateau forcing: I. Formation. Clim Dyn 39(5):1169–1181. https://doi.org/10.1007/s00382-012-1334-z

Yatagai A, Kamiguchi K, Arakawa O, Hamada A, Yasutomi N, Kitoh A (2012) APHRODITE constructing a long-term daily gridded precipitation dataset for Asia based on a dense network of rain gauges. Bull Am Meteorol Soc 93(9):1401–1415. https://doi.org/10.1175/Bams-D-11-00122.1

Ye BS, Yang DQ, Ding YJ, Han TD, Koike T (2004) A bias-corrected precipitation climatology for China. J Hydrometeorol 5(6):1147–1160. https://doi.org/10.1175/Jhm-366.1

Zadra A (2013) WGNE drag project: an inter-model comparison of surface stresses, edited. http://collaboration.cmc.ec.gc.ca/science/rpn/drag_project/documents/wgne_drag_project_report01.pdf

Zhang YC, Huang AN, Zhu XS (2006) Parameterization of the thermal impacts of sub-grid orography on numerical modeling of the surface energy budget over East Asia. Theor Appl Climatol 86(1–4):201–214. https://doi.org/10.1007/s00704-005-0209-1

Zheng DH, Van der Velde R, Su ZB, Wen J, Wang X, Booij MJ, Hoekstra AY, Lv SH, Zhang Y, Ek MB (2016) Impacts of Noah model physics on catchment-scale runoff simulations. J Geophys Res-Atmos 121(2):807–832. https://doi.org/10.1002/2015jd023695

Zhou X, Beljaars ACM, Wang Y, Huang B, Lin C, Chen Y, Wu H (2017) Evaluation of WRF simulations with different selections of sub-grid orographic drag over the Tibetan plateau. J Geophys Res-Atmos 122:7755–7771. https://doi.org/10.1002/2016JD026213

Zhou X, Yang K, Wang Y (2018) Implementation of a turbulent orographic form drag scheme in WRF and its application to the Tibetan Plateau. Clim Dyn 50(7–8):2243–2255. https://doi.org/10.1007/s00382-017-3677-y

Zhu ML, Yao TD, Yang W, Xu BQ, Wu GJ, Wang XJ (2018) Differences in mass balance behavior for three glaciers from different climatic regions on the Tibetan Plateau (vol 50, pg 3457, 2018). Clim Dyn 50(1–2):769–769. https://doi.org/10.1007/s00382-017-3915-3

Zuo ZY, Zhang RH, Zhao P (2011) The relation of vegetation over the Tibetan Plateau to rainfall in China during the boreal summer. Clim Dyn 36(5–6):1207–1219. https://doi.org/10.1007/s00382-010-0863-6